Applied Energy 279 (2020) 115882

Contents lists available at ScienceDirect

Applied Energy

journal homepage: www.elsevier.com/locate/apenergy

Reforming of diesel and jet fuel for fuel cells on a systems level: Steady-state and transient operation

Remzi Can Samsun *, Matthias Prawitz, Andreas Tschauder, Jan Meißner, Joachim Pasel, Ralf Peters

Forschungszentrum Jülich GmbH, Electrochemical Process Engineering (IEK-14), 52425 Jülich, Germany

HIGHLIGHTS

- Experimental study of a 28 kW_{th} fuel processor for integrated fuel cell systems.
- Conversion in the reformer and shift reactor maximized simultaneously.
- Fuel conversion higher than 99.95% using commercial diesel and jet fuel.
- CO concentrations lower than 1% at the anode inlet using all fuels.
- Target CO level achieved even during transient operation with frequent load changes.

GRAPHICAL ABSTRACT

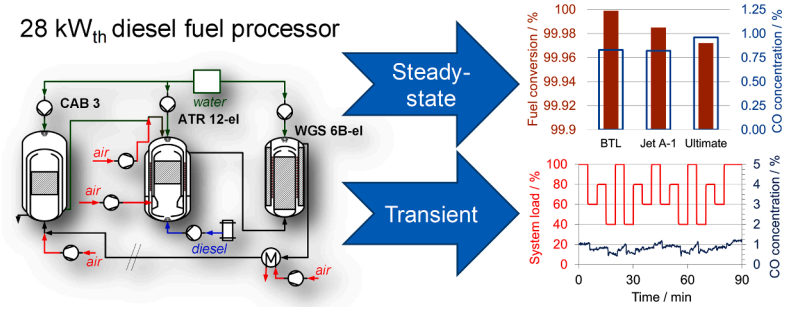

ARTICLE INFO

Keywords:
Auxiliary power unit
Fuel cell system
HT-PEFC
Jet A-1
Load change
Water–gas shift

ABSTRACT

The operation of fuel cell systems using liquid fuels widens the application possibilities of this promising energy conversion technology. However, systems utilizing diesel and jet fuel reforming are fairly complex and suffer from poor stability and limited dynamics. To address these challenges, this paper investigates the steady-state and transient operation of a 28 kW_{th} fuel processor on the systems level. With the help of experiments that make use of the developed prototype, suitable operating parameters are sought to maximize the simultaneous fuel conversion in the reformer and CO conversion in the shift reactor. Furthermore, a load change strategy is developed with the aim of keeping the CO concentration at the fuel cell anode inlet below the target concentration of 1% of the wet product gas at all times. The identified parameters enable very high conversions (>99.95%) and CO concentrations even lower than the target during steady-state operation using three commercial fuels under full load. The developed load change strategy was validated during 90 min tests, including 16 load change cycles with loads between 40% and 100%. As well as providing excess steam during load change, the selection and control of optimal O_2/C and H_2O/C ratios and temperature levels proved to be of key importance. In order to minimize the CO concentration, it is recommended to operate the reformer at the identified parameters for each fuel and keep the shift outlet temperature between 295 and 300 °C by adjusting the water feed. The proposed fuel processor concept and the experimentally-validated operating strategies in this work can enable the successful implementation of fuel cell technology in different application areas, including auxiliary power units, remote power systems and range extenders.

* Corresponding author.
E-mail address: r.c.samsun@fz-juelich.de (R.C. Samsun).

https://doi.org/10.1016/j.apenergy.2020.115882
Received 16 June 2020; Received in revised form 10 September 2020; Accepted 13 September 2020
Available online 29 September 2020

1. Introduction

The use of logistical fuels such as diesel and kerosene-type jet fuel in fuel cell systems extends the application possibilities of this promising energy conversion technology to areas where hydrogen infrastructure is not available or a hydrogen solution is difficult to implement due to volumetric or gravimetric restrictions. Possible application areas of fuel cells operated with diesel and kerosene reformate include auxiliary power units (APUs) for various means of transportation, including aircraft [1], trucks [2] and ships [3]; power supply systems for remote locations [4]; range extenders for electric vehicles [5]; propulsion systems for underwater applications [6]; freight locomotives [7]; and combined heat and power for ships [8]. The high efficiency and low emission potential of the fuel cell technology can then be combined with the extensive infrastructure of fossil-based diesel and jet fuel for short-term applications. In the mid- to long-term, synthetic liquid fuels produced via biomass-to-liquid or power-to-liquid processes also offer a sustainable energy conversion pathway as an additional advantage. Furthermore, diesel reforming can be employed to enhance efficiency and reduce the emissions of a diesel engine [9].

Despite considerable scientific and technological achievements in the last decade, which are reflected in the review articles listed in Table 1, the reforming of diesel and jet fuel still presents several challenges that restrain the widespread commercialization of fuel cell systems that utilize these fuels. These challenges include the time and energy required for start-up, system complexity, limited dynamics, volume, system stability and shut-down procedures, which will be discussed in the following sub-sections.

1.1. Start-up

Several publications focused on start-up at a systems level. Maximini et al. [15] applied oxidative steam reforming of diesel as a measure to actively heat the system components using the produced reformate. Han et al. [16] utilized H_2O_2 decomposition heat to reduce the start time for subsea applications where no oxygen is available. Samsun et al. proposed electrical [17] and thermal [18] start-up approaches for a diesel-based high-temperature PEFC system. All of these works provided experimentally-validated strategies at the systems level. Recently, using an electrical start strategy, Samsun et al. were able to achieve a 16 min start time for a sixth generation diesel fuel processor to reach full load operation with ideal reformate quality, suppressing side products [19]. This result is promising for achieving the 30 min target for the fuel cell system [20].

1.2. Shut-down

Like the start-up procedure, the shut-down of a reformate-based fuel cell system is not trivial. Krekel et al. [21] observed very high concentrations of by-products during shut-down and were able to reduce these by a factor of 400 thanks to advanced shut-down approaches. These approaches were further optimized, leading to the complete elimination of by-products during shut-down; furthermore, nitrogen was replaced by air as the purge gas and a regeneration procedure was implemented in the procedure [22].

Table 1
Selection of publications reviewing the progress on diesel and jet fuel reforming.

Author(s)	Focus	Source
Bae	Fuel processing of liquid fuels for SOFCs, including catalyst degradation, design aspects, post-processing and durability issues.	[10]
Wierbicki et al.	Jet fuel reforming, including catalyst system interactions, reaction kinetics and sulfur poisoning.	[11]
Xu et al.	Diesel and jet fuel reforming focused on ATR, including reaction thermodynamics, major issues, reactor design and operating strategies.	[12]
Bae et al.	Liquid fuel processing technologies and reactor concepts in the kW class.	[13]
Specchia	Fuel processing reactors and integrated systems for various fuel cell types focusing on products for APU and CHP applications in Europe.	[14]

1.3. System volume

The high number of components required to realize and operate the complete fuel processing routes leads to low power densities or integrated system architectures that are hard to control due to interactions between the system components. Ercolino et al. [23] and Cutillo et al. [24] evaluated the performance of different fuel processing routes and CO fine cleaning for PEFC systems by means of process analysis, whereas Walluk et al. [25] and Goell et al. [26] focused on the simulation of the combination of autothermal diesel reforming and SOFC technology, including off-gas recycling. Accounts of fuel cell operation with diesel reformate are limited in the literature. Jeong et al. [27] and Rautanen et al. [28] reported on experiments on the coupling of diesel reforming with an SOFC, whereas Engelhardt et al. [29] and Samsun et al. [30] with low- and high-temperature PEFC technology. Only a few publications in the literature list the volume of the components, as the reactors are developed for catalyst screening or are prototypes. A reactor's integration with a focus on the system aspects is undertaken in limited cases. Peters et al. [31] presented a methodology for developing integrated reformer designs with high power densities based on computational fluid dynamics. One example of this approach was the autothermal reformer ATR 12, which was characterized by Pasel et al. [32]. Meanwhile, Samsun et al. [19] integrated the second version of this reformer type in the sixth generation diesel fuel processing system, resulting in a high power density of 123 $W_{el}\ l^{-1}$. This reformer version also included a high-capacity electric heater and vapor trap analogous to the newest generation of reformers from Jülich, presented by Pasel et al. [33].

1.4. Load change

Another challenge addressed is the limited dynamics of a diesel fuel processing system during load change. As all reactors operate at their best on their design points, deviations from these during load change or operation at partial load can lead to an insufficient reformate quality. Several publications handled the load change strategy at a reactor level in recent years. Dolanc et al. focused on the control of an autothermal diesel reformer [34] and, respectively, an afterburner [35] for a diesel-based PEFC system. Their strategy is based on keeping the reactor temperatures at a set-point and controlling the hydrogen production rate for the reformer. In a simulation work, Malik et al. [36] implemented controllers to keep the catalyst temperature near set-points for achieving the desired hydrogen flow rate from an autothermal diesel reformer in a PEM fuel cell system. Peters et al. [37] and Pasel et al. [33] reported on load change experiments using NExBTL and Ultimate diesel, respectively, for a period of 75 h, including 10 load change sequences in total. Using a fuel injector in pulsed mode, they could achieve loads of between 20% and 100%. At the systems level, Samsun et al. [22] operated the fourth generation diesel fuel processor of Jülich in the APU mode of operation. Across three difficulty levels, a typical 5 h break of a heavy-duty truck was demonstrated with load change steps of between 40% and 80%. It was observed that during load increases to 80%, the target CO concentration at the anode inlet could not be achieved. In a theoretical study, Ipsakis et al. [38] simulated a fuel cell system with liquid fuel processing and showed that flexible operation and fast transients can be achieved through the proper selection of parameters. Bizon recently published on the load-following, control-based, real-time optimization of hybridized fuel cell systems [39].

1.5. Complexity of diesel reforming and stability issues

Finally, identifying the optimal combination of the catalyst system and operation parameters to produce a stable reforming performance has been the focus of many works on diesel reforming in recent years. Most of these publications report on catalyst stability, typically using surrogate diesel and low gas hourly space velocities (GHSV), while only a few focus on reactors. At the systems level, very few publications exist concerning stable operation. Creaser et al. published a kinetic model to describe the autothermal reforming of diesel using Rh-based catalysts [40]. Similarly, Dorazio and Castaldi [41] proposed a detailed reaction scheme for the autothermal reforming of tetradecane as a diesel surrogate using a Pt-based catalyst. Chen et al. [42] analyzed the reforming of commercial diesel with the help of experiments and simulations, showing that the deviation between diesel reformate composition and surrogate reformate composition using n-heptane/toluene is large. Therefore, they recommended using a multi-component surrogate to more accurately represent diesel. In order to decrease coke formation, eliminate coke deposition and reform the produced side products during diesel steam reforming, Arslan Bozdag et al. [43] reduced the GHSV to 7500 h^{-1}, increased the H_2O/C ratio and optimized their Ni-based catalyst with CeO_2 and tungsten. Tribalis et al. [44] demonstrated sulphur tolerance and stability during the steam reforming of surrogate diesel for 160 h at 20,000 h^{-1} by doping their Ni-based catalyst with La and Ba. Younis et al. [45] investigated Ni-based catalysts containing lanthanide series promoters for diesel steam reforming. The Pr-Ni catalyst showed the most promising results for 40 h at 5800 h^{-1} GHSV with low coke formation.

Xu et al. [46] identified bimetallic Ni/noble metal catalysts on hydrotalcite supports promoted by alkaline or rare earth materials as being the most promising systems for on-board reforming for APU applications in their review. Ju et al. [47] analyzed the influence of aromatic contents in the surrogate fuel for diesel and concluded that enhancing the Ni-based reforming catalyst with Rh slowed down the decrease in the catalytic performance. Zhang et al. [48] developed a Rh/NiO/K-La-Ce-Al-Ox catalyst and achieved 89% conversion during the autothermal reforming of desulphurized Jet A under optimal operating conditions. Fabiano et al. developed a steam reformer using a commercial Rh-based catalyst and achieved the full conversion of dodecane at a GHSV of 3500 h^{-1} [49]. O'Connell et al. attained 38 h of operation with a micro reactor in the 5 kW class during the steam reforming of diesel with at least 98% conversion and using commercial catalysts [50]. Studies by Shoynkhorova et al. [51–53] and Rogozhnikov et al. [54] focused on diesel reforming using Rh-containing catalysts prepared by sorption-hydrolytic deposition. Firstly, they demonstrated full conversion for the autothermal reforming of n-hexadecane for 12 h [51]. Then, they compared the catalytic activity of their Rh-based catalyst system with Pt- and Ru-based systems, finding that the Rh-based system had the highest activity. This catalyst showed stable performance during the autothermal reforming of summer diesel at a high GHSV of 30,000 h^{-1} for 9 h [52]. In another study, they brought this Rh-based composite catalyst onto a wire mesh honeycomb module and could demonstrate the full conversion of n-hexane at 10,000 h^{-1} and 98% at 13,300 h^{-1} during autothermal reforming [53]. Using the same catalyst system, a pilot scale reactor was built and tested for the autothermal reforming of diesel at 15,000 h^{-1}, resulting in complete conversion for 200 min [54]. Lo Faro et al. [55] analyzed the operation of an SOFC with reformate for the steam reforming of n-dodecane using an Rh-based catalyst at 16,000 h^{-1}. They observed cracking at low steam-to-carbon ratios of 1 and a decrease in cell performance at 1.5. The best performance was achieved at a steam-to-carbon ratio of 2. Nehter et al. [56] demonstrated the pre-reforming of road diesel for SOFC systems for maritime applications on a 0.9 kW scale. Lacking a regeneration procedure, the experiment was terminated after 3200 h due to a significant deactivation of the catalyst bed. Pasel et al. [57] operated a water–gas shift reactor with diesel reformate for 5000 h. The CO concentration at the shift reactor outlet could be kept under 1.5 (vol)% following the regeneration cycles. The reformate was produced in an autothermal diesel reformer operating at 20,000 h^{-1}.

Samsun et al. demonstrated the direct coupling of a reformer and shift reactor not only during steady-state operation, but also during start-up and shut-down [18,22]. Under worst case conditions, the CO concentration at the WGS outlet amounted to 1.5 (vol.)%, in parallel to increases in the CO concentrations at the reformer outlet using the fourth generation diesel fuel processor [22]. In the fifth generation diesel fuel processor [18], a good steady-state performance was observed, but full load operation was not possible due to non-matching reactor sizes. Moreover, high amounts of by-products were observed at the reformer outlet, making it difficult to identify suitable parameters for the stable operation of the shift reactor. Unfortunately, the applied technique to determine the amounts of by-products in the reformate showed a very high measurement uncertainty for benzene. Meißner et al. [58] proposed a new method that enables the detection of traces of hydrocarbons in the product gas from the autothermal reforming of middle distillates using GC/MS coupling.

1.6. Approach and background

Based on the short literature survey presented above, it can be concluded that the challenges to start-up and shut-down have been extensively discussed and have resulted in experimentally-validated solutions at a systems level. With respect to the system volume, integrated system designs with a high power density also exist. This paper deals with the three remaining challenges. On the one hand, the stability and complexity of these challenges is addressed. The target is to achieve operation at a high conversion with different commercial fuels at a systems level. The approach will aim to find suitable operation parameters with each fuel, despite the high level of system integration. Furthermore, load change strategies are developed and validated as a response to the third challenge, which is that of limited dynamics. In the previous system generation, the maximum power level of the system was limited to 50% due to the new design parameters of the shift reactor [18]. Here, a new shift reactor generation is utilized that is in the same power class as the other components. Therefore, the system can be operated at full load, exploiting the full potential of the reactors during operation at high gas hourly space velocities. The latter was a limitation in many of the published works presented above concerning stability, even at the catalyst or reactor levels. Furthermore, a new generation of reformers is employed that can achieve very high conversion, unlike the reactors used in earlier systems [18].

The novelty of the present work is therefore its uniqueness in addressing the identified challenges of diesel reforming at a systems level, in an effort to bridge the gap between research on catalysts and reactors and the application of integrated energy systems. It offers experimentally-validated, steady-state and transient operating strategies for the kW-class, integrated diesel fuel processing systems for optimal fuel cell operation. The basis of the work is a high-power density, self-sustaining diesel fuel processor in the 28 kW_{th} power class developed for high-temperature PEFC systems.

2. Experimental

For this study, the experiments were performed using the sixth generation diesel fuel processing system developed at Jülich. The main components of this system are an autothermal reformer (ATR), a water–gas shift reactor (WGS), a catalytic burner (CAB) and a heat exchanger. Fig. 1 presents a simplified sketch of this system to explain the coupling of the reactors with each other. A recent publication from our group reports on the start-up performance of this system generation and explains the components in detail [19]. As the system is developed for coupling with a high-temperature PEFC, a water–gas shift reactor is necessary to reduce the CO content of the reformate after the reformer.

The external heat exchanger conditions the hot reformate and cold cathode air before entering the fuel cell stack. The catalytic burner then processes the anode off gas to minimize the emissions.

2.1. System lay-out and preparation

As Fig. 1 indicates, the main components of the system include not only catalyst beds, but also mixing chambers and heat exchangers (see the legend for color descriptions). This is an approach to minimize the number of components and piping to connect them with each other on the one hand and to maximize the system efficiency in terms of recovering process heat on the other. However, as was mentioned in the introduction, this simultaneously increases the system's complexity, as a parameter change in one of the reactors directly influences the others.

As the name implies, autothermal reforming takes place in the reformer upon mixing superheated steam and air with liquid fuel. The catalyst bed, in the form of a monolith, is designed for a gas hourly space velocity (GHSV) of 30,000 h^{-1} at 100% load (2.7 kg h^{-1} fuel, molar O_2/C ratio of 0.47, H_2O/C ratio of 1.9), utilizing a commercial noble metal catalyst based on Rh/Pt. Superheated steam from the catalytic burner is first mixed up with air (air ATR steam) and, in a second mixing chamber at the other end of the reformer, with water (water ATR HEX). Based on the desired operation point of the reformer, the ratio between both water feeds (water ATR CAB/water ATR HEX) must be adjusted, keeping the total water amount for reforming constant based on the pre-set load level and molar H_2O/C ratio. The mixture of these three streams leads to a saturated water/air mixture, which is superheated in the ATR heat exchanger using the hot reformate. Similar to steam, the ratio between air fed through the heat exchanger via the steam path (air ATR steam) and cold air fed through the ATR mixing chamber (air ATR MC) must be adjusted, keeping the total air amount for reforming constant based on the pre-set load level and molar O_2/C ratio. The high-temperature shift stage of the WGS reactor has a GHSV of 45,000 h^{-1} and is fed directly with ATR reformate cooled in the ATR heat exchanger. Thus, the inlet temperature of the WGS reactor can only be tuned through the operating parameters of the ATR. After the first conversion step of CO and H_2O into H_2 and CO_2 in the high-temperature shift stage, the input of additional water (water WGS) not only cools the reformate for the low-temperature shift stage (22,500 h^{-1}), but also enhances the thermodynamic equilibrium of the shift reaction towards the products of H_2 and CO_2. For both shift steps, a Pt-based commercial noble metal catalyst is used. Both stages are housed in a cylindrical reactor where the high-temperature shift stage is placed in the center of the reactor and the low-temperature shift stage is situated in the outer section, surrounding the high-temperature part. The stages are separated by a hollow volume through which the product gas of the high-temperature stage is directed to the low-temperature stage after the addition of water. After heat treatment in the external heat exchanger, the reformate is fed into the fuel cell anode. During the tests conducted for this study, the reformate is sent instead to the catalytic burner in order to close the heat balance of the system and thus simulate the anode off gas. As the reformate gas has a much higher calorific value than the anode rest gas, the air amount for catalytic combustion (air CAB) is kept so low that a comparable amount of heat supply is enabled. As is mentioned above, the catalytic burner and reformer are also thermally coupled to each other, as part of the water demand of the reformer is supplied through the CAB heat exchanger (water ATR CAB) in the form of superheated steam. Similar to other reactors, a commercial noble metal catalyst based on Pt/Rh is used and is coated in a ceramic monolith.

The reactors were designed based on the pressure equipment directive (PED) of the European Union with the support of computational fluid dynamics (CFD) simulations and analyses that employed the finite element method (FEM). Following the computer-aided design (CAD), the reactors were manufactured in the Central Institute for Engineering and Technology (ZEA-1) of the Forschungszentrum Jülich. Nozzles for water and diesel supply to the reactors and catalyst systems were purchased as commercial products. The fuel processor system was designed in the basic engineering phase with the help of process simulations. The detailed engineering phase consisted of diagrams and plans that provide information for the selection of pipes and other balance of plant components. The system packaging was realized with the help of CAD. After the procurement of all additional components, the fuel processor package was assembled and assigned the CE mark of conformity. For characterization, the system was docked on a test rig that was developed for the testing of fuel processors.

2.2. Reaction mechanism

The main reactions taking place in the fuel processor are outlined in Table 2. Autothermal reforming is normally a combination of catalytic

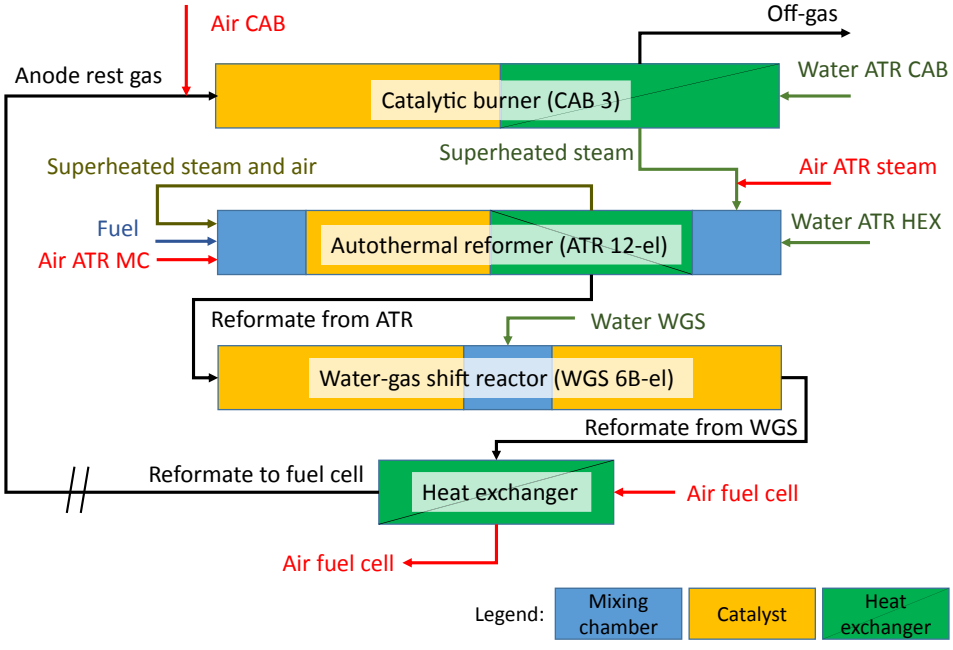

Fig. 1. Simplified sketch of the diesel fuel processing system, including the coupling of the reactors to each other.

partial oxidation (2) and steam reforming (5), accompanied by simultaneous equilibrium reactions for water–gas shift (6) and both methanation reactions (7), (8). Some sources use a combination of total oxidation (1) and steam reforming (5) in order to describe autothermal reforming. The highest temperature observed at the inlet of the catalyst bed is normally higher than the maximum adiabatic temperature that can be achieved by partial oxidation. Creaser et al. [40] suppress partial oxidation in their reaction scheme in order to achieve high catalyst temperatures at the inlet with the help of total oxidation; however, at the same time they state that partial oxidation also takes place in practice. From an energy balance point of view, both routes result in an identical temperature and product gas composition following autothermal reforming. The only difference is in the intermediate temperature observed following the fast oxidation at the catalyst inlet. In practice, it can be expected that both total and partial oxidation occur during autothermal reforming, as the high temperatures measured at the catalyst inlet can only be achieved by total oxidation and there is clear evidence in the literature that partial oxidation is observed during autothermal reforming. Dorazio and Castaldi [24] propose a detailed mechanism for the autothermal reforming of tetradecane using 24 reactions, which are classified under C_{14} reactions, water consuming reactions, hydrocarbon oxidation and hydrocarbon intermediate reactions. According to their experimentally-supported analysis, the reactions' sequence commences with oxidation and cracking reactions, but the dominant reactions are primarily partial oxidation and, to a lesser degree, the water–gas shift reaction. Speight [59] points out equation (3) as the general reaction equation without catalyst for thermal partial oxidation where CO and H_2O are produced from the partial combustion of a sub-stoichiometric fuel–air mixture. It must be noted, that this equation is slightly modified here to close the atomic balance. Similarly, Yoon et al. [60] discuss the total oxidation equation (1) taking place before reaching the catalyst bed where most of the diesel is decomposed and a large quantity of ethene is produced. Another equation (4) for partial oxidation is proposed by Kang et al. [61], where CO_2 and H_2 are produced. A more complicated reaction equation for partial oxidation is reported by Bae et al. [13], in which not only CO and H_2 are produced as in the simplified equation for catalytic partial oxidation (2), but also CO_2 as in equation (4) and H_2O as in equation (3). The water–gas shift reaction (6) is responsible for a higher rate of conversion of steam than steam reforming, leading to a similarly high concentration of carbon dioxide as carbon monoxide in the reformate. Typical methane values in the product gas for reforming and the overall stoichiometric balance show that CO methanation (7) takes place to a limited extent and that the effect of CO_2 methanation (8) can be neglected in the balance. In addition, during partial oxidation of n-dodecane under 600 °C, Bae et al. [13] show that CO_2 and CH_4 are the main products. Xu et al. [12] propose a reaction mechanism for autothermal reforming based on partial oxidation and steam reforming, declaring ethene as the main reason for rapid carbon formation citing Yoon et al. [60] who found out that ethene pyrolysis is homogenous and takes place at the reactor entrance. According to these experiments, insufficient steam leads to performance degradation and lack of oxygen in the downstream leads to ethene formation, favoring ATR against steam reforming and partial oxidation. The important conclusion of Xu et al. is that the control of H_2O/C and O_2/C ratios in the inlet mixture of reforming plays an essential role in the suppression of carbon formation.

The water–gas shift reaction (6), taking place as a desired side reaction in the reformer, occurs as the main reaction in the water–gas shift reactor in the abovementioned catalyst system. Due to the well-known character of this reaction, namely the high equilibrium conversions at low temperatures and good reaction kinetics at high temperatures, the water–gas shift reactions occur at two temperature levels in the designed water–gas shift reactor. Finally, the remaining calorific compounds of carbon monoxide, hydrogen and methane in the anode rest gas are combusted according to CO (9), H_2 (10) and CH_4 (11) oxidation reactions in the catalytic burner.

Table 2
The main reactions taking place in the fuel processor.

Reaction	Chemical formula *Jet A-1: n = 12, m = 24;* *Ultimate diesel: n = 19, m = 38;* *NExBTL diesel: n = 17, m = 36;*	Reactor (s)	Eq. number
Total oxidation	$C_nH_m + (n + m/4)\ O_2 \rightarrow n\ CO_2 + m/2\ H_2O$	ATR	(1)
Partial oxidation	$C_nH_m + n/2\ O_2 \rightarrow n\ CO + m/2\ H_2$	ATR	(2)
	$C_nH_m + (2n + m)/4\ O_2 \rightarrow n\ CO + m/2\ H_2O$		(3)
	$C_nH_m + n\ O_2 \rightarrow n\ CO_2 + m/2\ H_2$		(4)
Steam reforming	$C_nH_m + n\ H_2O \rightarrow n\ CO + (m/2 + n)\ H_2$	ATR	(5)
Water-gas shift	$CO + H_2O \leftrightarrows CO_2 + H_2$	ATR, WGS	(6)
CO methanation	$CO + 3\ H_2 \leftrightarrows CH_4 + H_2O$	ATR	(7)
CO_2 methanation	$CO_2 + 4\ H_2 \leftrightarrows CH_4 + 2\ H_2O$	ATR	(8)
CO oxidation	$CO + 0.5\ O_2 \rightarrow CO_2$	CAB	(9)
H_2 oxidation	$H_2 + 0.5\ O_2 \rightarrow H_2O$	CAB	(10)
CH_4 oxidation	$CH_4 + 2\ O_2 \rightarrow CO_2 + 2\ H_2O$	CAB	(11)

2.3. System characterization

In an attempt to simulate the real application character as much as possible, the system is not pre-heated or prepared by other means before each experiment. Instead, it is started from cold mode using the newly developed electrical start-up strategy [19] in each experiment. In the slowest case, the start-up procedure is completed in 22 min, leading to self-sustaining, full load operation. The shut-down is performed according to the already published procedure, which leads to neither higher hydrocarbon content nor temperature peaks [22]. Moreover, a regeneration with air at the end of each experiment is integrated into the shut-down procedure. The steady-state and load change experiments were performed during operating periods of at least 6 h between regular start-up and shut-down experiments.

The experiments are carried out with the help of a process control system and the produced gases are analyzed continuously after water separation using FTIR/MS coupling. Details of the specific experimental techniques can be found in Samsun et al. [18]. The products of the experiments are the measured temperatures, pressures, flow rates and product gas concentrations. The changes to these parameters are recorded every 1–10 s according to the type of experiment and transferred to Excel sheets for further evaluation. To analyze the concentrations of undesired by-products, the newly-developed GC/MS method of Meißner et al. [58] is used, which reduces the detection limit of the analytics to the sub-ppm range. The conversion calculation is based on the methodology presented in Samsun and Peters [62], although it excludes the carbon in the condensed phase, which cannot be analyzed due to integrated system operation. The excluded amount is typically one order of magnitude lower than the carbon present in the gas phase. Unless otherwise stated, all concentrations are given in the dry state.

In the first part, focus is given to determining the best possible operating parameters to maximize conversion in the reformer and, at the same time, to minimize the CO content at the outlet of the shift reactor at maximum load, which represents the worst case. No defined limits for the undesired by-products are cited in the literature. Krekel et al. investigated the stability of the WGS catalysts using synthetic diesel reformate containing 220 ppmv higher hydrocarbons and observed no negative effects [21]. On the fuel cell level, Engelhardt et al. operated their HT-PEFC at a stable cell voltage for 16 h using diesel reformate, which contained 2500–3300 ppmv residual hydrocarbons at a fairly low current density of 0.2 A cm^{-2} [29]. However, Bae et al. define ethene as a carbon precursor and state that deactivations in diesel reforming catalysts are accompanied by the production of light hydrocarbons such as ethene [13]. Therefore, in this work the aim is to suppress the

production of undesired by-products to the greatest extent possible. For reforming, NExBTL diesel from Neste, desulphurized Jet A-1 and Aral Ultimate diesel are used to represent different diesel and jet fuels from various origins and complexities in relation to their end of boiling and aromatic content. More detail on the properties of these fuels can be found in the literature [63].

In the second part, a load change strategy is developed and optimized, and is then validated using each fuel with the aim of keeping the CO concentration at the shift outlet below the target concentration of 1.25 (vol.)% in the dry state, corresponding to 1 (vol.)% in the wet state. Although the HT-PEFC anode can tolerate higher CO concentrations of up to 3 (vol.)% [64], the target concentration for both parts of this work is set to the concentrations stated above, in order to minimize the drop in cell voltage and maximize cell efficiency during each operation sequence.

3. Results and discussion

The results are presented in two sections. The first focuses on steady-state experiments, while the second concentrates on transient operation.

3.1. Optimization of steady-state performance

The first stage of the steady-state experiments was performed using NExBTL diesel fuel. This fuel can be considered the simplest in this paper, as it does not contain any aromatics. Based on a series of orientation experiments, the operating parameters for the reformer were selected as molar ratios of $O_2/C = 0.47$ and $H_2O/C = 1.9$, with a ratio of cold air to pre-heated air of 70:30 (air ATR MC/air ATR HEX, see Fig. 1) and a ratio of cold water to superheated water of 32:68 (water ATR HEX/water ATR CAB, see Fig. 1). All steady-state experiments in this paper were carried out using 2.7 kg h^{-1} of fuel, corresponding to 100% load. In the first experiment (BTL I), the WGS water feed was defined as 2250 g h^{-1} and the air feed to the CAB as 7500 l_N h^{-1}. Afterwards, four additional experiments were performed in a narrow parameter window, varying the WGS water feed between 2200 and 2300 g h^{-1} and the air amount to the CAB between 7500 and 7600 l_N h^{-1}. The variation of the WGS water amount changes the temperature level and feed composition in the low-temperature shift stage. In turn, the variation in the air amount to the CAB changes the amount of heat release in the catalytic burner, which is recovered for educt conditioning in the reformer. Firstly, the concentrations of undesired by-products analyzed using GC/MS at the reformer outlet are given in Fig. 2. To give a better overview, the sum of all undesired by-products is also given in the form of total carbon on the right axis, which adds up the concentration of each by-product after multiplying the concentration with the corresponding carbon number. Operation with the lower air amount to CAB in experiments (BTL I, III and IV) led to lower by-products than operation with the higher air amount in experiments (BTL II and V). However, the difference is very low (1.38–3.32 ppmv vs 4.77–8.45 ppmv) and all operating parameters led to very high conversions (99.996–99.999%).

In principle, a higher amount of air to the CAB leads to higher temperatures in the reformer, which in turn helps achieve higher conversion with better fuel evaporation. However, a high temperature level in the reformer also carries disadvantages. Pasel et al. [65] recommend keeping the reforming temperature as low as possible (< 900 °C) in order to maintain the redox properties of the catalyst and to prevent sintering of the catalyst particles. Therefore, it is crucial to find the optimum temperature level of the reformer, which is directly influenced by the operating conditions of the remaining reactors in the system. Here, with selected parameters, the optimal settings were already available for perfect fuel evaporation in the reformer. Therefore, additional heat input had no positive effect on the current set-up.

In a second analysis, the resulting CO concentrations at the WGS outlet were investigated for the same set of experiments. On the basis of the overall heat balance of the system and the resulting temperatures, as well as the cooling effect caused by the water feed at the outlet of the high-temperature shift stage, different temperature and conversion levels were observed in the WGS reactor. A clear trend can be observed if the CO concentrations at the WGS outlet are analyzed together with the outlet temperature of the WGS reactor, as presented in Fig. 3. If the results from the five experiments are analyzed together, it can be seen that within the analyzed operation window, the outlet temperature of the WGS was decisive for the CO concentration at the WGS outlet: the lower the reformate temperature at the WGS outlet, the higher the CO conversion, resulting in a lower CO concentration. At the resulting window of temperatures of between 311 °C and 329 °C, the reaction was not yet limited by kinetics, such that higher conversions were achieved at lower temperatures, in agreement with thermodynamic equilibrium.

The final goal is to observe if there is a correlation between the amount of by-products and the achieved CO concentrations in the WGS reactor. The lowest amounts of by-products were observed for experiments BTL I and III, whereas the highest CO concentrations were also observed in these. As a result, it can be concluded that in this very narrow window of operating conditions, it cannot be concluded that the amount of by-products in the ATR reformate has a direct effect on the performance of the WGS reactor.

In all five experiments, each performed for a period of six hours,

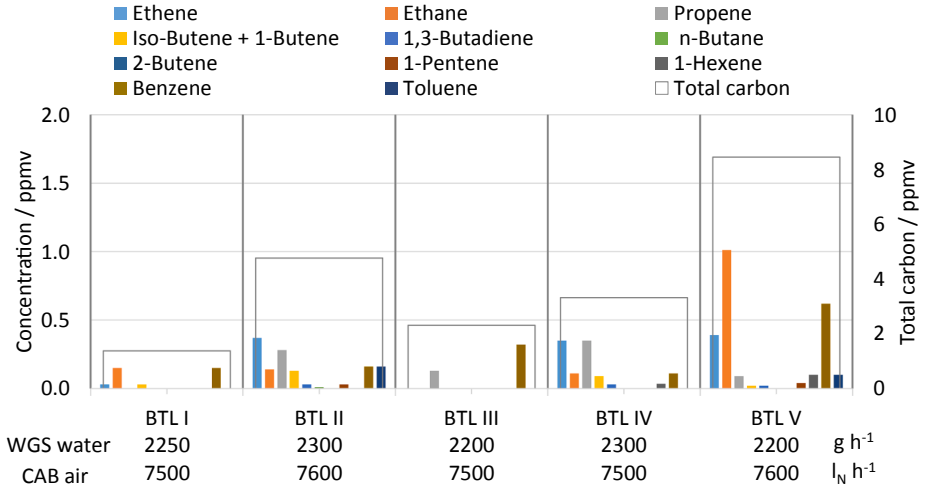

Fig. 2. Concentrations of undesired by-products (left axis) and the total amount of carbon from undesired by-products (right axis) at the reformer outlet using 2.7 kg h^{-1} NExBTL diesel.

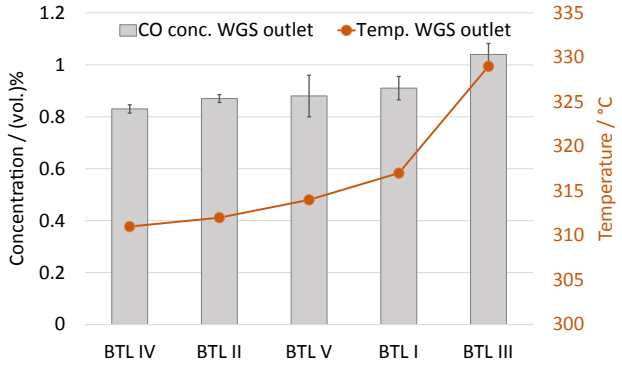

Fig. 3. Mean values of CO concentrations at the WGS outlet with their standard deviations (left-axis) in correlation with the outlet temperature of the WGS reactor (right-axis) using 2.7 kg h^{-1} of NExBTL diesel. The experiments have been arranged in the order of increasing outlet temperature.

there was no degradation observed during the experiment or after the controlled shut-down procedure and the new start. In addition, all five experiments offered parameter combinations, which led to very low CO concentrations at the WGS outlet (0.83–1.04 (vol.)%) and very low amounts of by-products in the reformer outlet (1.38–8.45 ppmv) during operation at full load, which is the extreme case for the later application.

In the second step, the steady-state operation was extended to desulphurized Jet A-1 and Aral Ultimate diesel. Due to their aromatic content, these fuels are more difficult to reform in comparison to NExBTL diesel, which lacks an aromatic content.

The reference experiment using desulphurized Jet A-1 was JA II, with the same molar ratios (O_2/C = 0.47, H_2O/C = 1.9) and proportions (air ATR MC/ATR HEX = 70:30, water ATR HEX/ATR CAB = 32:68) as in the NExBTL experiments. In addition, the CAB air amount was set to 7400 l_N h^{-1} and the WGS water amount to 2600 g h^{-1} for JA II after the first orientation experiments. As a slight increase in the concentrations of the single by-products and the total carbon amount was observed in this experiment, in comparison to the experiments BTL I-V, a parameter variation was performed. Experiment JA I was intended to reduce the heat input to the reformer in the form of superheated steam from the CAB, and therefore the ratio of water from the CAB was reduced from 68% in JA II to 63%. In order to ensure lower heat input, the CAB air amount was also reduced to 7200 l_N h^{-1}. Otherwise, the temperature of the superheated steam would increase for the same amount of released heat in the catalytic burner and transfer a comparable amount of heat to the reformer. In a third experiment, JA III, the higher heat input case was simulated, increasing the ratio of CAB water to 74% and the CAB air quantity to 7600 l_N h^{-1}. All of the other parameters were kept identical to those in JA II. In a final experiment, JA IV, an extreme parameter combination was simulated in accordance with the parameters from the last system generation, which resulted in the stable operation of the system with the highest conversion using desulphurized Jet A-1 [18]. Accordingly, the molar O_2/C ratio was set to 0.49, the ratio of CAB water to 60% and the CAB air feed to 7000 l_N h^{-1}. All other parameters were kept identical to those in experiment JA II. Fig. 4 shows the concentrations of by-products for each experiment.

Surprisingly, neither an increase in heat input to the reformer in JA III nor a reduction in JA I led to fewer by-products than the reference experiment JA II. Going to a higher molar O_2/C ratio and lower CAB water ratio, as well as CAB air feed in JA IV to suppress the strong temperature increase in the reformer due to the higher O_2/C ratio, also did not improve the conversion. The colder operation phase in JA I resulted in the highest concentrations for ethane and benzene, which made the total carbon amount higher than 100 ppmv. In JA III, the higher heat input resulted in a slight increase in ethene and benzene concentrations and so the total carbon concentration increased from 34 ppmv in JA II to 48 ppmv. The best-of point from the previous system generation in JA IV did not improve the conversion in comparison to JA II or JA III. However, the concentrations of by-products were still much lower than those achieved with the previous system generation [18].

The lowest CO concentration (0.79 (vol.)%) at the WGS outlet was measured in JA I at the lowest outlet temperature of the WGS (275 °C), despite it having the highest amount of by-products. Interestingly, the CO concentration achieved at JA II (0.82 (vol.)%) is fairly comparable to this value, although the temperature was somewhat higher, at 302 °C. This shows that the operation of the WGS at even lower temperatures does not carry a large advantage. Due to slower reaction kinetics, higher CO conversions enabled by thermodynamic equilibrium could not be reached.

The highest CO concentration (0.98 (vol.)%) was observed with JA III at the highest outlet temperature of 324 °C, one of the operating points with fewer by-products. Again, no correlation was observed between the amount of by-products at the reformer outlet and the CO conversions in the WGS reactor. The latter seems to only be determined

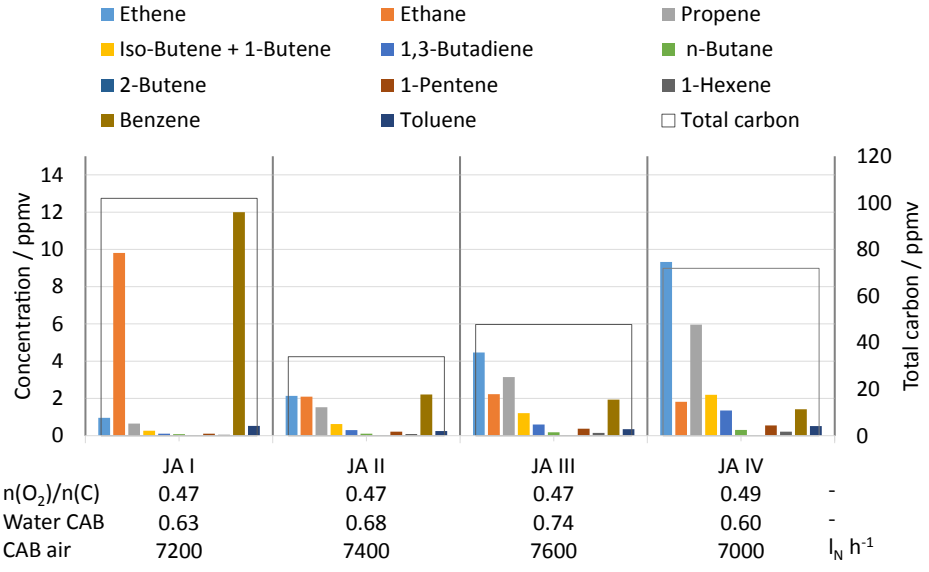

Fig. 4. Concentrations of undesired by-products (left axis) and the total amount of carbon from undesired by-products (right axis) at the reformer outlet using 2.7 kg h^{-1} of desulphurized Jet A-1.

by the temperature level for the experiments performed in this section. Finally, JA II offered the most advantageous operating parameters, resulting in the highest conversion (99.985%), and at the same time a fairly low CO content at the WGS outlet (0.82 (vol.)%) at full load.

Similarly, the reference experiment with Ultimate diesel was ULT II, where identical parameters of molar ratios (O_2/C = 0.47, H_2O/C = 1.9) and proportions (air ATR MC/ATR HEX = 70:30, water ATR HEX/ATR CAB = 32:68), as in the NExBTL experiments and JA II, were selected. In this case, the CAB air amount was set to 7500 l_N h^{-1} and the WGS water amount to 2400 g h^{-1} after the first orientation experiments. Similar to the variation in experiments JA I-III, the heat input to the reformer was reduced (ULT I) and increased (ULT III). Again, the best-of point from the previous system generation for Ultimate diesel [18] was investigated in ULT IV. Fig. 5 presents the concentrations of undesired by-products and the total carbon produced by experiments ULT I-IV, together with the varied parameters. Looking at the selected parameters, it can be observed that the WGS water feed could not be kept constant in all experiments, unlike experiments JA I-IV. In experiments ULT III and IV, the amount of water was increased to reduce the CO concentrations at the WGS outlet, in conjunction with the higher temperature level in the system, due to selected parameter combinations. It should also be noted that the parameters in ULT IV differed strongly from those in JA IV. As mentioned before, the parameters were taken from the previous generation. Therein, it was mandatory to implement this set of extreme parameters in order to achieve a stable system operation with the target CO concentrations.

The results in Fig. 5 show that the operating parameters, leading to an increased heat input to the reformer in ULT III in comparison to the reference case in ULT II, could slightly reduce the total amount of carbon from 68 ppmv to 65 ppmv. In contrast, operation at lower heat input in ULT I again resulted in higher quantities of by-products. It would be interesting to increase the CAB water ratio further to see if an additional reduction can be achieved. However, this is not realistic, as with its present design, the catalytic burner cannot provide more heat during anode off-gas operation without reducing the hydrogen utilization rate in the fuel cell. Yet, the ULT IV experiment offered another possibility to shift the temperature level higher without facing this limit. In this experiment, the O_2/C and H_2O/C ratios were increased while the CAB water ratio was decreased. At the same time, the complete amount of ATR air was fed into the reformer after being pre-heated in the ATR heat exchanger. However, the largest amount of total carbon, and thus the lowest level of conversion, was achieved in this experiment. Therefore, the ULT III experiment offered the lowest amount of by-products in total amongst the experiments carried out for this paper with Ultimate diesel, showing a 99.972% conversion at full load during system operation. At the same time, benzene concentration was at the lowest level (2.72 ppmv) during ULT III.

Once again, no direct correlation between the CO conversion in the WGS and the amount of by-products at the reformer outlet could be observed. Experiments ULT I and ULT IV showed CO concentrations of between 0.73 and 0.80 (vol.)% at outlet temperatures of between 296 and 299 °C, whereas ULT II and ULT III resulted in 0.94–0.96 (vol.)% at 313–315 °C. Apart from this general trend, which is fully in agreement with experimental results obtained using NExBTL diesel and desulphurized Jet A-1, the direct correlation between the outlet temperature and the resulting CO concentration was not observed here. Despite its lower temperature ULT I showed a higher concentration than ULT IV. The same effect is also observed between ULT III and ULT II, whereas in that case the difference was negligible. Comparing the experimental conditions between ULT I and ULT IV, it can be observed that the reformer was operated at a higher steam-to-carbon ratio in ULT IV than in the other experiments. As a direct result, the CO concentration at the reformer outlet dropped from 11 to 11.2 (vol.)% to 10.1 (vol.)%. Finally, the lowest CO concentration, of 0.73 (vol.)%, was achieved in ULT IV, which is also the lowest value achieved in this paper. Although operation at a higher steam-to-carbon ratio did not bring an advantage concerning the fuel conversion in the reformer, the use of higher steam-to-carbon ratios with more appropriate parameters can be further investigated in future work. Arslan Bozdag et al. reported decreased coke formation and increased WGS activity through an increase in the steam-to-carbon ratio [43].

This paper also shows that in the case of a reformer enabling high fuel conversions with very low amounts of by-products, such as the one used in this work, it is not necessary to adopt extreme parameter combinations (see JA IV and ULT IV). Such combinations were required in the previous reformer generation [18] in order to minimize the amount of by-products and achieve stable performance in terms of fuel and CO conversion in the reformer and shift reactor. In this work, the application of the same parameters resulted in a lower amount of by-products than those of the former reformer generation [18]; however, the resulting values were not superior to those in experiments JA II and ULT III.

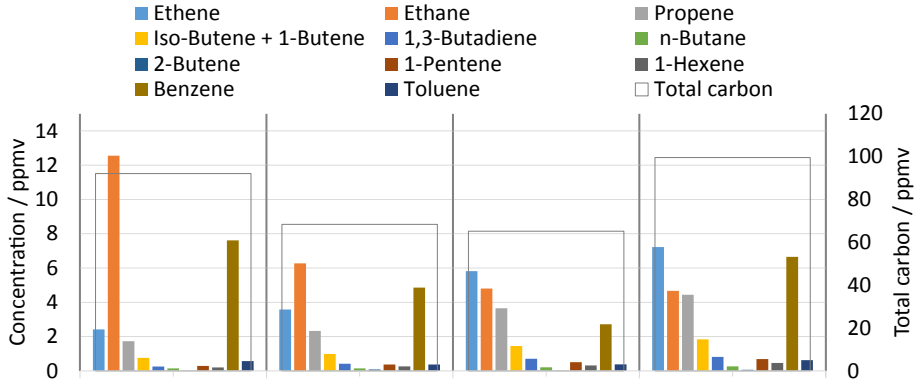

	ULT I	ULT II	ULT III	ULT IV	
$n(O_2)/n(C)$	0.47	0.47	0.47	0.49	-
$n(H_2O)/n(C)$	1.90	1.90	1.90	2.10	-
Water CAB	0.63	0.68	0.74	0.66	-
Air cold	0.70	0.70	0.70	0.00	-
WGS water	2400	2400	2700	2800	g h^{-1}
CAB air	7200	7500	7750	7800	l_N h^{-1}

Fig. 5. Concentrations of undesired by-products (left axis) and the total amount of carbon from undesired by-products (right axis) at the reformer outlet using 2.7 kg h^{-1} Ultimate diesel.

Finally, this section showed that by using the selected parameter combinations, it was possible to minimize the concentrations of undesired by-products and keep the total carbon concentration below 10 ppmv in all experiments using NExBTL diesel. During system operation with desulphurized Jet A-1, it was observed that the total carbon concentration could be reduced down to 34 ppmv by means of the identified parameters. Similarly, during operation with Ultimate diesel, the total carbon concentration could be reduced to 65 ppmv. Comparing the sum of concentrations for ethene and ethane with those from the former reformer generation [18] shows a reduction of these undesired by-products of 94% using NExBTL diesel, 70% using desulphurized Jet A-1 and 81% using Ultimate diesel. The stable operation of the reforming process can be explained by the optimal design and operating parameters. The reformer's mixing chamber is designed with the purpose of enabling the proper mixing of the educts. This was a measure against the well-known mechanism of pyrolysis, which leads to ethene formation due to improper mixing [13]. In addition, the selection of the optimum O_2/C and H_2O/C ratios for each fuel, which is known to play an essential role in the suppression of carbon formation [12], has proven itself to be an effective approach to achieving a stable steady-state performance in this work. This is driven by the overall motivation defined in the beginning, which was to minimize the concentrations of higher hydrocarbons in the reformate. Fundamentally, autothermal reforming has intrinsic advantages over steam reforming and partial oxidation due to the presence of both steam and oxygen in the feed gas. According to the literature, the addition of even small amounts of air prevents the onset of deactivation processes [50], whereas high O_2/C ratios may even enable effective coke suppression [13]. The selected optimum O_2/C ratio in this work is fairly high, at 0.47, and is close to the maximum value of 0.5, which is the maximum limit for partial oxidation. The disadvantage of a low hydrogen yield during operation at high O_2/C ratios is countered with an accompanying high H_2O/C ratio of 1.9. This ratio enables high CO conversions in the water–gas shift reaction, increasing the hydrogen yield in the reformate. As the preparation of superheated steam for reforming required no external heat, operation at a high H_2O/C ratio has no disadvantage for the level of efficiency. The integration of a regeneration strategy into the shut-down procedure was another component of the effective operating strategy in this work.

In addition, during all of the experiments performed, the selected parameter combinations led to CO concentrations in the range of 0.73–1.04 (vol.)% at the outlet of the WGS reactor during full load operation for 6 h during each experiment. This performance can be explained by three effects. First, the stable performance of the upstream reforming process led to an ideal educt mixture for the water–gas shift reaction. Secondly, the selected parameters for reformer operation with each fuel could deliver an ideal inlet temperature for the high-temperature shift stage, in which the higher share of CO could already be converted into CO_2 with the help of good reaction kinetics at higher temperatures. At the same time, the temperature level was low enough to prevent catalyst degradation, e.g., due to sintering. Finally, in the low-temperature shift stage, an ideal temperature window for the reactor outlet was identified, in which the CO concentrations only depended on the thermodynamic equilibrium and were not limited by poor reaction kinetics, which is typical at low temperatures.

To summarize, it was possible to identify parameter combinations for each fuel to maximize the fuel conversion at the reformer outlet and keep the CO concentration at the WGS outlet well below the target value of 1.25 (vol.)%, also during system operation at full load.

3.2. Optimization of transient operation

The aim of the experiments in this section was to optimize transient operation. As mentioned in the previous section, due to the high level of system integration, the interactions between the components limit flexibility in operation. This is not only the case during steady-state operation, but also during transient operation, as the parameters and resulting conditions in the components deviate strongly from the design values during these periods. In this section, load change strategies were developed with the help of experiments to minimize the load change periods and ensure smooth system operation at all times. This section is composed of three sub-sections. Firstly, orientation experiments were performed to understand the dynamics of the system. This was followed by a 90 min test based on a pre-defined load cycle. Finally, the developed load change strategy was validated using the same fuels as were used for steady-state operation.

3.2.1. Orientation experiments

The orientation experiments were performed using NExBTL diesel with the standard molar O_2/C and H_2O/C ratios and air and water ratios for the reformer as in experiments BTL I-V. The system load was varied between 40% as the minimum value and 100% as the maximum. The system parameters were controlled in such a way that the load was given as input, and only the remaining flow rates of diesel, air, and water were adjusted as a function of the load for the pre-defined values mentioned above. There were no further disturbances to the components, as self-sustaining operation was achieved at all times without any external heat input.

In the first load change experiment LC I, the water feed to the reformer was adjusted manually during load increases due to the slow reaction time of the control loop of water feed. This means that the control value of the particular controller was entered by hand during load increase. In order to determine the control values for each load point, the system was operated at different load levels prior to the experiment and the resulting control value for each controller was read for the desired load point. For the air and fuel flows, a fast and precise reaction of the control loops was observed, so a manual adjustment was not required for these flows. During load reduction, water, air and fuel flows were adjusted automatically, whereas a 1 s delay time was introduced for air and fuel flows. Furthermore, the load change was achieved in stepwise changes of 10 percentage points.

In the second load change experiment LC II, the delay time for air and fuel was set to 5 s in order to allow enough time for the water feed to adjust itself during both the load increase and decrease. No manual adjustment was performed. Additionally, instead of stepwise load changes, instant load changes were performed.

In the final orientation experiment LC III, the delay time was again reduced to 1 s during the load decrease and the water feed was adjusted manually during load increase. Similar to LC II, instant load changes were performed. Fig. 6 presents the recorded flow rates in the system and the measured product gas concentrations at the WGS outlet during the load change experiments.

Fig. 6a shows four load changes between 100% and 40% for a period of 60 min in experiment LC I. The stepwise load change resulted in a long period until the desired new load levels were achieved. For example, during a load increase from 40% to 100%, the new load level was achieved after 245 s with 2% tolerance (deviation from the new load level) and, after 249 s, with 1% tolerance. Similarly, during a load reduction from 100% to 60%, the new load level was achieved after 112 s with 2% tolerance and 122 s with 1%. As presented in Fig. 6b, the product gas compositions at the WGS outlet remained stable during the entire test period, with slight deviations. The CO concentration at the WGS outlet remained under the target value of 1.25 (vol.)% the entire time, ensuring fuel cell operation under ideal conditions.

In LC II, the switch to instant load changes resulted in smooth load changes, which can be seen in Fig. 6c. Here, four load changes are presented for a period of 30 min. Moreover, the course of concentrations show a stable trend in Fig. 6d. Similar to LC I, the CO concentration remained well below the target value during the entire experiment. Using the instant load change strategy, the load change sequences were strongly accelerated. During load increase from 40% to 100%, the new load level was achieved after 24 s (2%) to 33 s (1%). A load reduction from 100% to 60% was realized after 36 s (2%) to 47 s (1%).

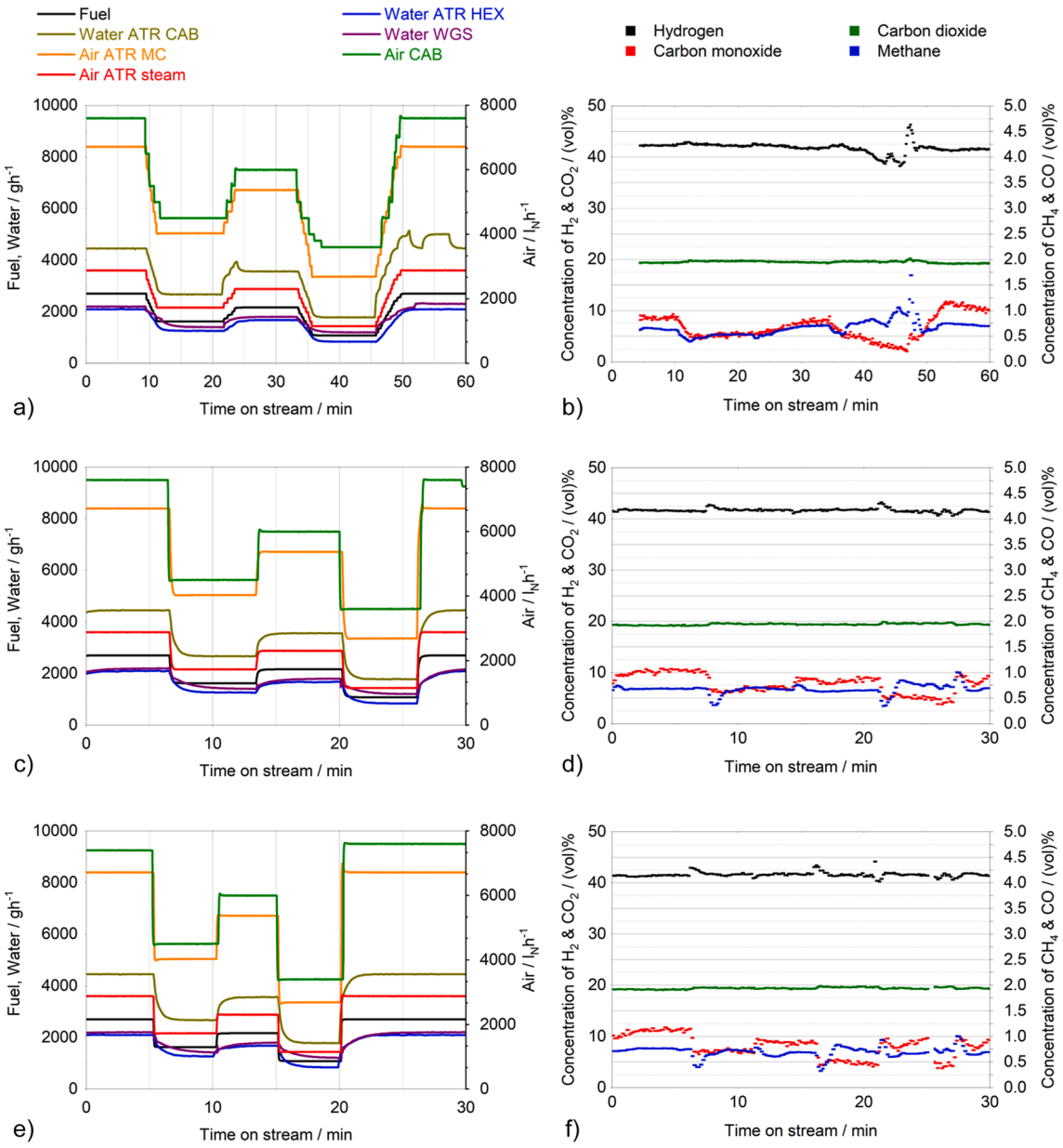

Fig. 6. Results of load change experiments LC I (a, b), LC II (c, d) and LC III (e, f) with NExBTL diesel. Left: Flow rates of fuel, air and water in the system. Right: Concentrations of H_2, CO_2, CO and CH_4 at the WGS outlet.

As mentioned above, a combination of the advantages of both strategies was tested in LC III. The instant load change approach resulted in a course of flow rates in Fig. 6e that is similar to that in Fig. 6c. The course of the product gas concentrations was also stable, with the CO concentration remaining below the target value at all times. However, LC III resulted in a further reduction in the load change periods in comparison to LC II. A load increase from 40% to 100% was achieved after 18 s (2%) to 20 s (1%). Meanwhile, a stronger reduction was observed in the load reduction from 100% to 60%, with 13 s (2%) to 17 s (1%).

The orientation experiments in LC I-III showed that the instant load change strategy led to a strong reduction in the load change period. Instead of a 5 s delay time for air and diesel, it was more advantageous to keep the delay time at 1 s and increase the water feed manually during load increase, as practiced in LC III.

3.2.2. 90 min test based on a pre-defined load cycle

In this section, the optimum load change strategy that was identified in the previous section (see experiment LC III) was applied for a pre-defined load cycle for 90 min. In this experiment, the aim was to test the above-developed strategy for more frequent load changes for a longer period of time. During the experiments in the previous section, it was observed that the greatest challenge arose during load increase from 40% to 100%. The pre-defined cycle in experiment LC IV therefore included twice the load changes, from 100% to 40% and 40% to 100%. Furthermore, a load change was performed every 5 min, resulting in 16 load change sequences in 90 min. The results of this experiment, carried out using NExBTL diesel with standard parameters, are presented in Fig. 7.

For the sake of better presentation, the air and water streams to the ATR are grouped to single curves in Fig. 7a. As the water feed was adjusted manually during load increase and automatically during load decrease, the course of the water flow rates reached their set points after a certain delay during load decrease. In these transient periods, the system was operated with larger water amounts than the design points, which did not lead to a disturbance of the system operation. In such

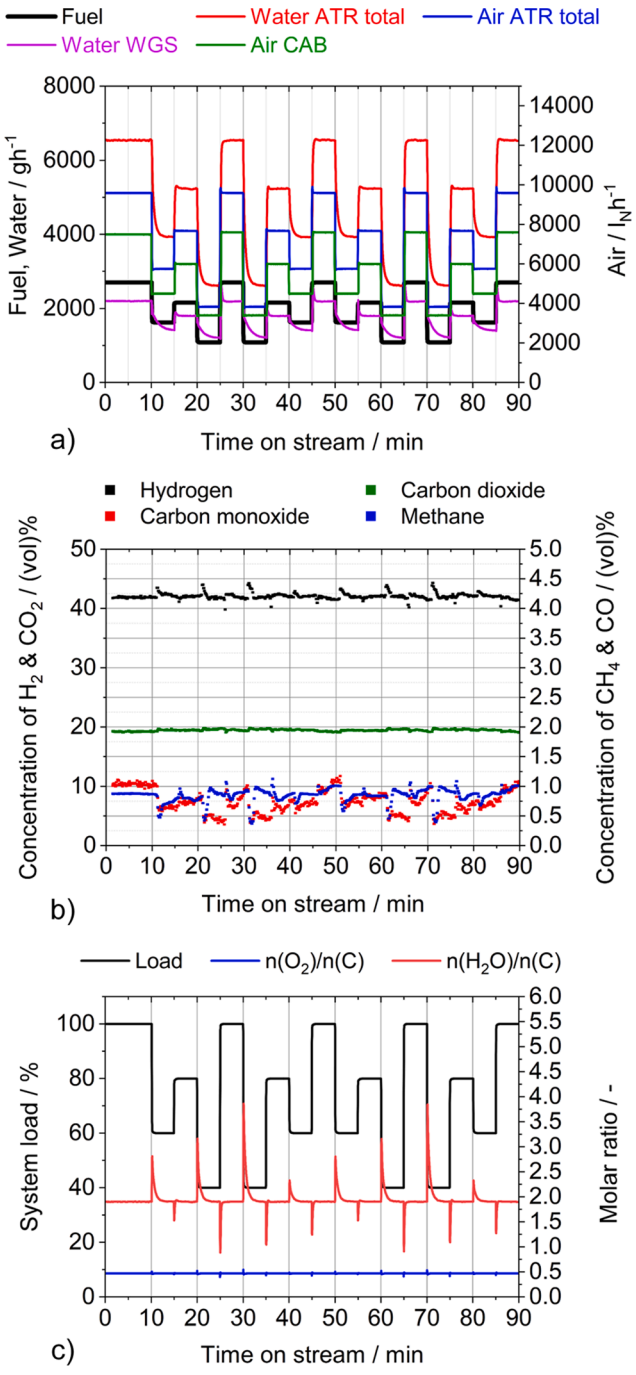

Fig. 7. (a) Educt flow rates in the system; (b) concentrations of H_2, CO, CO_2 and CH_4 at the WGS outlet; and (c) system load and molar ratios O_2/C and H_2O/C in the reformer in experiment LC IV using NExBTL diesel.

periods, a short-term increase in the hydrogen concentration is observed in Fig. 7b, which also shows that the target CO concentration of 1.25 (vol.)% was never exceeded in this load change experiment.

For a deeper analysis of the experimental results, an additional chart is plotted that presents the molar oxygen-to-carbon and steam-to-carbon ratios in the reformer, together with the system load in Fig. 7c. In the ideal case, these molar ratios should remain constant at the pre-defined values of 0.47 (O_2/C) and 1.9 (H_2O/C). According to Fig. 7c, the oxygen-to-carbon ratio was kept fairly tight at the desired set point. Due to the aforementioned slow reaction time of the water pumps during load decrease, major deviations from the set points were observed after each load decrease, which is in agreement with the observation made above, in Fig. 7a, and can be considered as uncritical. However, Fig. 7c also shows that despite the manual adjustment of the water feed during load increase, which is much faster than automatic adjustment, the steam-to-carbon ratio dropped to 1.0 for very short time periods. As steam acts as an inhibitor against the formation of carbonaceous deposits during reforming, even such short periods with an undersupply of steam must be avoided with a better control strategy.

On the basis of this finding, a time resolution analysis of the results was performed to determine the weakness of the applied control strategy. This analysis showed that the following step increases occured during load increase: 1. Load; 2. ATR water; 3. CAB water; 4. WGS water; 5. CAB air. It is clear that the water feed to the reformer through the ATR HEX and CAB (see Fig. 1) in steps 2 and 3 must be initiated before load, in other words a fuel increase. Additionally, the CAB air feed must be increased before load increase to provide the CAB with enough air all the time. Similarly, the load decrease was realized in the following sequence: 1. CAB air; 2. load (including water and air for the ATR); 3. WGS water. As mentioned above, the operation of the reformer with the excess water does not disturb the reforming process, as enough excess heat is available during load change from higher load levels to lower ones. Yet, the CAB air feed should also only be reduced after load reduction to sustain a complete combustion of the anode off-gas during load change.

Based on these findings, the control loops for load increase and decrease sequences were modified. According to the optimized strategy, the following steps are defined to achieve load increase under ideal conditions: 1. ATR water; 2. CAB water; 3. CAB air; 4. Load; 5. WGS water. For load reduction, the new strategy defines: 1. Load; 2. CAB air; 3. ATR water; 4. CAB water; 5. WGS water.

3.2.3. *Validation of the new load change strategy*

In this sub-section, the new load increase and decrease strategies developed in the previous sub-section were validated using the same pre-defined load cycle as in experiment LC IV. For this purpose, three experiments were performed using NExBTL diesel (LC V), desulphurized Jet A-1 (LC VI) and Ultimate diesel (LC VII). All three of these were carried out with the reference parameters of molar $O_2/C = 0.47$ and $H_2O/C = 1.9$, a ratio of cold air to pre-heated air of 70:30 and a ratio of cold water to superheated water of 32:68. For the sake of simplicity, the experimental results are discussed using two diagrams for each experiment in Fig. 8. On the left-hand side, the system load and molar ratios in the reformer are presented for each experiment, whereas the resulting concentrations of H_2, CO_2, CO and CH_4 at the WGS outlet are presented on the right-hand side. An initial look into the curves of the left-hand size, generated based on the educt flow rates, shows that the pre-defined load change cycle was realized for each fuel. Moreover, the strong reductions of the steam-to-carbon ratios beyond the set point at 1.9 could be completely avoided with the new strategy.

Similarly, the course of the measured concentrations at the WGS outlet was very stable for each experiment. Using NExBTL diesel (LC V) and des. Jet A-1 (LC VI), the measured CO concentrations were kept below the target value of 1.25 (vol.)% during the complete load change experiment. Only in the final experiment (LC VII) with Ultimate diesel did the two measurement points, out of 5400 (90 min × 60 measurements/min), lay slightly higher than the 1.25 (vol.)% target with 1.26 (vol.)% and 1.28 (vol.)%. Interestingly, these values were not measured during the most critical load increase steps from 40% to 100%, but instead at a more moderate step during load increase, from 40% to 80%. Finally, it can be concluded that the target CO concentration was only slightly exceeded for a period of 1 s each, which should not lead to a remarkable change in fuel cell performance, given that it is possible to run an HT-PEFC with a CO concentration of 3 (vol)% without damage or degradation.

The analysis of the example load increase and decrease periods is also summarized in Table 3. In addition to the example load change periods analyzed in the orientation experiments, the most critical load

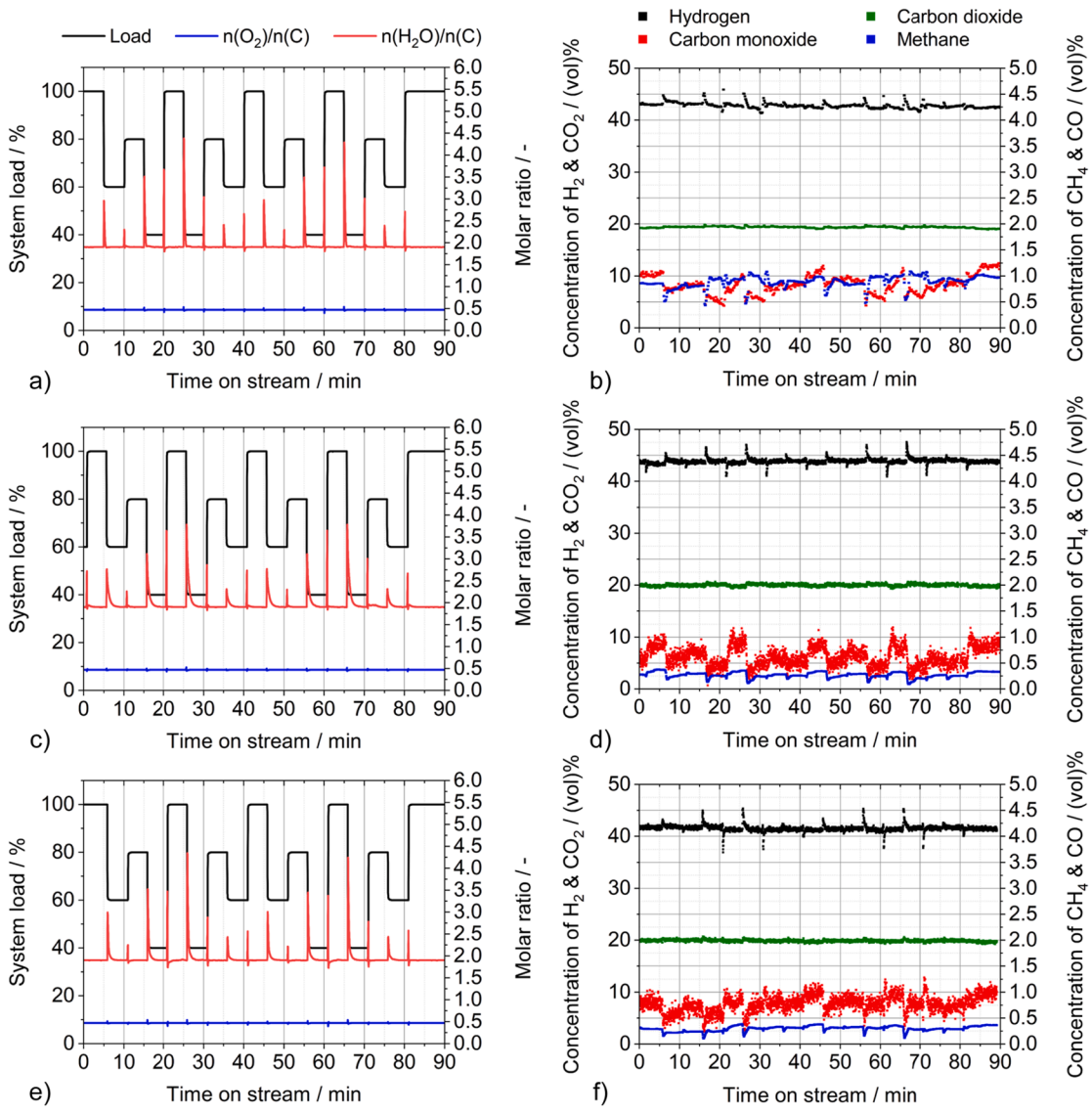

Fig. 8. Left: System load and molar ratios O_2/C and H_2O/C in the reformer in (a) exp. LC V using NExBTL diesel (c) exp. LC VI using des. Jet A-1 (e) exp. LC VII using Ultimate diesel. Right: Concentrations of H_2, CO, CO_2 and CH_4 at the WGS outlet in the LC V (b), LC VI (d) and LC VII (f).

reduction step, from 100% to 40%, is also analyzed. The analysis results show that a typical load increase from the minimum (40%) to maximum (100%) load was realized after 16 s considering 2% tolerance and 18 s considering 1% tolerance with all of the fuels. These values are almost identical to those from experiment LC III. A typical load decrease from 100% to 60% took 8 s (2%) to 16 s (1%), which is also not slower than orientation experiment LC III. Therefore, the optimized load change strategy is not only advantageous in terms of avoiding an undersupply of steam for the stable operation of the reformer and air for the low-emission catalytic burner operation in the final system, but also does not lead to a delay in the load change period. The analysis of the final load reduction step from 100% to 40% required 12 s (2%) to 24 s (1%). The increased period, in comparison to the 100–60% example, can be explained by the increased step size.

Table 3
Example load change periods for validation experiments LC V-VII.

Experiment	Example load change period (2%/1%)		
	Load increase 40% → 100%	Load reduction 100% → 60%	Load reduction 100% → 40%
LC V: NExBTL diesel	16 s/17 s	8 s/13 s	12 s/22 s
LC VI: des. Jet A-1	16 s/18 s	9 s/16 s	14 s/24 s
LC VII: Ultimate diesel	16 s/17 s	8 s/14 s	12 s/21 s

3.3. Discussion

The stable performance of the water–gas shift reactor during the load change experiments can be attributed to the fact that the upstream reformer was operated under optimal conditions, not only during steady-state operation but also during transient periods. The developed load change strategy enables proper mixing at all times to overcome the challenge of improper mixing and the pyrolysis and poor evaporation during load change it can lead to [13]. The presence of an abundance of steam for the reforming prior to load increases, together with precise control of the O_2/C ratio with the proposed load change strategy, ensured proper control of the steam and oxygen quantities. As was already mentioned, the control of the H_2O/C and O_2/C ratios of the feed gases played an essential role in the suppression of carbon formation in the literature [12], which proved itself to be the key control parameter

in the load change strategy followed in this work. As observed during the steady-state experiments, the excessive amount of steam in the reformer inlet had a positive effect on the equilibrium composition of the water–gas shift reaction (6) at the outlet of the water–gas shift reactor. Higher H_2O/C ratios than the design value of 1.9 result in lower CO concentrations, as the equilibrium of reaction (6) was shifted towards the CO_2 and H_2 products. In addition, improved reforming catalyst durability was reported at higher H_2O/C ratios in the literature [13], which can be attributed to effective ethene suppression.

It was also observed in this work that the water–gas shift reactor has the capacity to keep the target CO concentration at its outlet for changing upstream feed compositions and temperatures across a broad range of conditions, e.g., during steady-state operation with different fuels or transient operation during load changes. This feature can be ascribed to the innovative design of the reactor. The previous shift reactor concepts consisted of two adiabatic reactors and showed a very limited extent of operational flexibility. The new shift reactor is also operated without external cooling, but its special geometry, explained in section 2.1, enables an indirect cooling of both shift stages. Instead of a classical temperature increase along the reactor's length during an exothermic reaction in an adiabatic reactor, the temperature profile here first shows an increase but then decreases when approaching the outlet. Such a profile makes use of the faster reaction kinetics at high temperatures and the higher equilibrium conversions for CO at low temperatures in both shift stages at different temperature levels.

4. Conclusions

Instead of a laboratory-scale reactor or catalyst test, or the inline testing of several fuel processing reactors, an integrated fuel processor with a high power density (123 $W_{el}\ l^{-1}$) and application-oriented power class (28 kW_{th}) was developed. Moreover, instead of surrogate fuels, commercial diesel and jet fuels were used in the reformer at a high GHSV of 30,000 h^{-1}, which resulted in high conversions (>99.95%) during system operation. The target CO concentration was achieved for smooth coupling with a high-temperature PEFC stack during steady-state and transient operation with the developed strategies, which consist of the best set of parameters for steady-state and load change strategies during transient operation.

Each of the 13 steady-state experiments presented in this paper for periods of six hours, with different fuels, demonstrate APU operation at maximum load, which is typically not the case in real applications, as the system is not operated at full load all the time. Yet, the selected parameters for each fuel enabled very high conversions in the reformer and CO concentrations even lower than 1 (vol)% at the shift outlet (cf. target CO concentration: 1.25 (vol)%). In the previous system generation, maximizing the reformer conversion was unfortunately coupled with higher reformer temperatures and thus higher inlet temperatures in the WGS, which resulted in increased CO concentrations at the WGS outlet. With the present reactor generations, it was possible to maximize both conversion levels at the same time, despite the reformer operation having halved the residence time. This was not only enabled by the improved reforming performance, but also by the resulting temperature profile in the WGS. Differing from the adiabatic WGS concept in all of the previous fuel processor generations, the new WGS concept integrated two shift stages under one reactor shell.

It was observed that the outlet temperature of the WGS is decisive for CO conversion in the temperature window between 295 and 330 °C. In this window, a direct correlation was observed between the temperature and CO concentration, which corresponds to thermodynamic equilibrium. Operation at even lower temperatures, such as 275 °C, does not reduce the CO concentration further at the same extent, due to limitations in reaction kinetics at lower temperatures. Therefore, keeping the shift outlet temperature at about 295–300 °C seems to be a good control target for future system operation, which can be easily realized by the control of water feed to the WGS. Operation of the WGS at increased residence times at partial loads can enable lower CO concentrations at lower temperatures. Similarly, it was observed that even lower CO contents can be achieved at the shift outlet if the reformer is operated at higher H_2O/C ratios. As fuel cell operation at lower CO concentrations has a direct influence on the cell voltage and in turn the system efficiency, it is worth exploring these possibilities with future system simulations and experiments.

The new load change strategy enabled keeping the target CO concentration not only during steady-state, but also during transient operation, despite frequent load changes and harsh load change steps. At the same time, critical operating conditions, such as avoiding an undersupply of water for reforming or air for the catalytic burner, were eliminated. During the most challenging load change steps, the new load levels were achieved within 18 s (load increase) to 24 s (load decrease), with a tolerance of 1%. These results show that the developed fuel processor could even be operated under transient mode with frequent load changes, despite its high level of system integration and the resulting interactions between the components.

Finally, it can be concluded that the developed operating strategies for steady-state and transient operation of an integrated diesel fuel processor could be successfully demonstrated using three different commercial diesel and jet fuels in this work. This system design and the developed strategies flow into a complete fuel cell APU, which is currently under development. Steady-state and transient operation strategies developed and validated in this work are crucial for the successful implementation of the fuel processing technology in different application areas, including auxiliary power units, remote power systems and range extenders. The experimentally-verified strategies also deliver important parameters for future modeling studies, which often lack experimental validation.

CRediT authorship contribution statement

Remzi Can Samsun: Conceptualization, Methodology, Writing - original draft. **Matthias Prawitz:** Validation, Investigation. **Andreas Tschauder:** Validation, Investigation. **Jan Meißner:** Formal analysis, Investigation. **Joachim Pasel:** Resources, Writing - review & editing. **Ralf Peters:** Funding acquisition, Writing - review & editing.

Declaration of Competing Interest

The authors declare that they have no known competing financial interests or personal relationships that could have appeared to influence the work reported in this paper.

Acknowledgements

The authors are especially grateful to the fuel processing department at the Forschungszentrum Jülich, with special thanks to Lydia Lang and Uwe Klüttgen for their technical support and Franziska Thimm for support in the product gas analysis. This study did not receive any specific grant from funding agencies in the public, commercial, or not-for-profit sectors.

References

[1] Peters R, Samsun RC. Evaluation of multifunctional fuel cell systems in aviation using a multistep process analysis methodology. Appl Energy 2013;111:46–63.
[2] Pregelj B, Micor M, Dolanc G, Petrovcic J, Jovan V. Impact of fuel cell and battery size to overall system performance – A diesel fuel-cell APU case study. Appl Energy 2016;182:365–75.
[3] Valadez Huerta G, Álvarez Jordán J, Dragon M, Leites K, Kabelac S. Exergy analysis of the diesel pre-reforming solid oxide fuel cell system with anode off-gas recycling in the SchIBZ project. Part I: Modeling and validation. Int J Hydrogen Energ 2018;43:16684–93.
[4] DePippo K, Peppley BA. Canadian remote community power generation: How reformer and fuel cell systems compare with diesel generators. Int J Energy Res 2019;43:1161–70.

[5] Tribioli L, Cozzolino R, Chiappini D, Iora P. Energy management of a plug-in fuel cell/battery hybrid vehicle with on-board fuel processing. Appl Energy 2016;184:140–54.
[6] Han G, Lee S, Bae J. Diesel autothermal reforming with hydrogen peroxide for low-oxygen environments. Appl Energy 2015;156:99–106.
[7] Martinez AS, Brouwer J, Samuelsen GS. Comparative analysis of SOFC–GT freight locomotive fueled by natural gas and diesel with onboard reformation. Appl Energy 2015;148:421–38.
[8] Bensaid S, Specchia S, Federici F, Saracco G, Specchia V. MCFC-based marine APU: Comparison between conventional ATR and cracking coupled with SR integrated inside the stack pressurized vessel. Int J Hydrogen Energy 2009;34:2026–42.
[9] Chuahy FDF, Kokjohn SL. High efficiency dual-fuel combustion through thermochemical recovery and diesel reforming. Appl Energy 2017;195:503–22.
[10] Bae J. Chapter 8 – Fuel processor lifetime and reliability in solid oxide fuel cells. In: Brandon NP, Ruiz-Trejo E, Boldrin P, editors. Solid oxide fuel cell lifetime and reliability. Academic Press; 2017. p. 145–71.
[11] Wierzbicki TA, Lee IC, Gupta AK. Recent advances in catalytic oxidation and reformation of jet fuels. Appl Energy 2016;165:904–18.
[12] Xu X, Li P, Shen Y. Small-scale reforming of diesel and jet fuels to make hydrogen and syngas for fuel cells: A review. Appl Energy 2013;108:202–17.
[13] Bae J, Lee S, Kim S, Oh J, Choi S, Bae M, et al. Liquid fuel processing for hydrogen production: A review. Int J Hydrogen Energy 2016;41:19990–20022.
[14] Specchia S. Fuel processing activities at European level: A panoramic overview. Int J Hydrogen Energy 2014;39:17953–68.
[15] Maximini M, Engelhardt P, Brenner M, Beckmann F, Moritz O. Fast start-up of a diesel fuel processor for PEM fuel cells. Int J Hydrogen Energy 2014;39:18154–63.
[16] Han G, Bae M, Cho S, Bae J. Start-up strategy of a diesel reformer using the decomposition heat of hydrogen peroxide for subsea applications. J Power Sources 2020;448:227465.
[17] Samsun RC, Krupp C, Tschauder A, Peters R, Stolten D. Electrical start-up for diesel fuel processing in a fuel-cell-based auxiliary power unit. J Power Sources 2016;302:315–23.
[18] Samsun RC, Prawitz M, Tschauder A, Pasel J, Pfeifer P, Peters R, et al. An integrated diesel fuel processing system with thermal start-up for fuel cells. Appl Energy 2018;226:145–59.
[19] Samsun RC, Prawitz M, Tschauder A, Pasel J, Peters R, Stolten D. An autothermal reforming system for diesel and jet fuel with quick start-up capability. Int J Hydrogen Energy 2019;44:27749–64.
[20] Spendelow JS, Papageorgopoulos DC. Application requirements/targets for fuel cell APUs. In: Stolten D, Samsun RC, Garland N, editors. Fuel cells: data, facts and figures. Weinheim: Wiley-VCH; 2016. p. 197–201.
[21] Krekel D, Samsun RC, Pasel J, Prawitz M, Peters R, Stolten D. Operating strategies for fuel processing systems with a focus on water-gas shift reactor stability. Appl Energy 2016;164:540–52.
[22] Samsun RC, Krekel D, Pasel J, Prawitz M, Peters R, Stolten D. A diesel fuel processor for fuel-cell-based auxiliary power unit applications. J Power Sources 2017;355:44–52.
[23] Ercolino G, Ashraf MA, Specchia V, Specchia S. Performance evaluation and comparison of fuel processors integrated with PEM fuel cell based on steam or autothermal reforming and on CO preferential oxidation or selective methanation. Appl Energy 2015;143:138–53.
[24] Cutillo A, Specchia S, Antonini M, Saracco G, Specchia V. Diesel fuel processor for PEM fuel cells: Two possible alternatives (ATR versus SR). J Power Sources 2006;154:379–85.
[25] Walluk MR, Lin J, Waller MG, Smith DF, Trabold TA. Diesel auto-thermal reforming for solid oxide fuel cell systems: Anode off-gas recycle simulation. Appl Energy 2014;130:94–102.
[26] Göll S, Samsun RC, Peters R. Analysis and optimization of solid oxide fuel cell-based auxiliary power units using a generic zero-dimensional fuel cell model. J Power Sources 2011;196:9500–9.
[27] Jeong J, Baek SW, Bae J. A diesel-driven, metal-based solid oxide fuel cell. J Power Sources 2014;250:98–104.
[28] Rautanen M, Halinen M, Noponen M, Koskela K, Vesala H, Kiviaho J. Experimental study of an SOFC stack operated with autothermally reformed diesel fuel. Fuel Cells 2013;13:304–8.
[29] Engelhardt P, Maximini M, Beckmann F, Brenner M, Moritz O. Coupled operation of a diesel steam reformer and an LT- and HT-PEFC. Int J Hydrogen Energy 2014;39:18146–53.
[30] Samsun RC, Pasel J, Janßen H, Lehnert W, Peters R, Stolten D. Design and test of a 5kWe high-temperature polymer electrolyte fuel cell system operated with diesel and kerosene. Appl Energy 2014;114:238–49.
[31] Peters R, Pasel J, Samsun RC, Scharf F, Tschauder A, Stolten D. Heat exchanger design for autothermal reforming of diesel. Int J Hydrogen Energy 2018;43:11830–46.
[32] Pasel J, Samsun RC, Tschauder A, Peters R, Stolten D. Advances in autothermal reformer design. Appl Energy 2017;198:88–98.
[33] Pasel J, Samsun RC, Meißner J, Tschauder A, Peters R. Recent advances in diesel autothermal reformer design. Int J Hydrogen Energy 2020;45:2279–88.
[34] Dolanc G, Pregelj B, Petrovčič J, Pasel J, Kolb G. Control of autothermal reforming reactor of diesel fuel. J Power Sources 2016;313:223–32.
[35] Dolanc G, Pregelj B, Petrovčič J, Samsun RC. Control of an afterburner in a diesel fuel cell power unit under variable load. J Power Sources 2017;338:117–28.
[36] Malik FR, Tieqing Z, Kim Y-B. Temperature and hydrogen flow rate controls of diesel autothermal reformer for 3.6 kW PEM fuel cell system with autoignition delay time analysis. Int J Hydrogen Energy 2020. https://doi.org/10.1016/j.ijhydene.2020.07.208.
[37] Peters R, Pasel J, Samsun RC, Scharf F, Tschauder A, Müller M, et al. Spray formation of middle distillates for autothermal reforming. Int J Hydrogen Energy 2017;42:16946–60.
[38] Ipsakis D, Ouzounidou M, Papadopoulou S, Seferlis P, Voutetakis S. Dynamic modeling and control analysis of a methanol autothermal reforming and PEM fuel cell power system. Appl Energy 2017;208:703–18.
[39] Bizon N. Real-time optimization strategies of Fuel Cell Hybrid Power Systems based on Load-following control: A new strategy, and a comparative study of topologies and fuel economy obtained. Appl Energy 2019;241:444–60.
[40] Creaser D, Karatzas X, Lundberg B, Pettersson LJ, Dawody J. Modeling study of 5 kWe-scale autothermal diesel fuel reformer. Appl Catal A 2011;404:129–40.
[41] Dorazio L, Castaldi MJ. Autothermal reforming of tetradecane (C14H30): A mechanistic approach. Catal Today 2008;136:273–80.
[42] Chen H, Wang X, Pan Z, Xu H. Numerical simulation and experimental study on commercial diesel reforming over an advanced Pt/Rh three-way catalyst. Catalysts 2019;9:590.
[43] Arslan Bozdag A, Deniz Kaynar AD, Dogu T, Sezgi NA. Development of ceria and tungsten promoted nickel/alumina catalysts for steam reforming of diesel. Chem Eng J 2019;377.
[44] Tribalis A, Panagiotou GD, Bourikas K, Sygellou L, Kennou S, Ladas S, et al. Ni catalysts supported on modified alumina for diesel steam reforming. Catalysts 2016;6:11.
[45] Younis MN, Malaibari ZO, Ahmad W, Ahmed S. Hydrogen production through steam reforming of diesel over highly efficient promoted Ni/γ-Al2O3 catalysts containing lanthanide series (La, Ce, Eu, Pr, and Gd) promoters. Energ Fuel 2018;32:7054–65.
[46] Xu X, Liu X, Xu B. A survey of nickel-based catalysts and monolithic reformers of the onboard fuel reforming system for fuel cell APU applications. Int J Energy Res 2016;40:1157–77.
[47] Ju DG, Jo SB, Ha DS, Kim TY, Jung SY, Chae HJ, et al. Enhanced Ni-Al-based catalysts and influence of aromatic hydrocarbon for autothermal reforming of diesel surrogate fuel. Catalysts 2019;9:573.
[48] Zhang S, Wang X, Xu X, Li P. Hydrogen production via catalytic autothermal reforming of desulfurized Jet-A fuel. Int J Hydrogen Energy 2017;42:1932–41.
[49] Fabiano C, Italiano C, Vita A, Pino L, Laganà M, Recupero V. Performance of 1.5 Nm^3/h hydrogen generator by steam reforming of n-dodecane for naval applications. Int J Hydrogen Energy 2016;41:19475–83.
[50] O'Connell M, Kolb G, Schelhaas KP, Schuerer J, Tiemann D, Ziogas A, et al. Development and evaluation of a microreactor for the reforming of diesel fuel in the kW range. Int J Hydrogen Energy 2009;34:6290–303.
[51] Shoynkhorova TB, Rogozhnikov VN, Simonov PA, Snytnikov PV, Salanov AN, Kulikov AV, et al. Highly dispersed Rh/Ce0.75Zr0.25O2-δ-η-Al2O3/FeCrAl wire mesh catalyst for autothermal n-hexadecane reforming. Mater Lett 2018;214:290–2.
[52] Shoynkhorova TB, Simonov PA, Potemkin DI, Snytnikov PV, Belyaev VD, Ishchenko AV, et al. Highly dispersed Rh-, Pt-, Ru/Ce0.75Zr0.25O2–δ catalysts prepared by sorption-hydrolytic deposition for diesel fuel reforming to syngas. Appl Catal B 2018;237:237–44.
[53] Shoynkhorova TB, Rogozhnikov VN, Ruban NV, Shilov VA, Potemkin DI, Simonov PA, et al. Composite Rh/Zr0.25Ce0.75O2-δ-η-Al2O3/Fecralloy wire mesh honeycomb module for natural gas, LPG and diesel catalytic conversion to syngas. Int J Hydrogen Energy 2019;44:9941–8.
[54] Rogozhnikov VN, Kuzin NA, Snytnikov PV, Potemkin DI, Shoynkhorova TB, Simonov PA, et al. Design, scale-up, and operation of a Rh/Ce0.75Zr0.25O2-δ-η-Al2O3/FeCrAl alloy wire mesh honeycomb catalytic module in diesel autothermal reforming. Chem Eng J 2019;374:511–9.
[55] Lo Faro M, Trocino S, Zignani SC, Italiano C, Vita A, Aricò AS. Study of a solid oxide fuel cell fed with n-dodecane reformate. Part II: Effect of the reformate composition. Int J Hydrogen Energy 2017;42:1751–7.
[56] Nehter P, Wildrath B, Bauschulte A, Leites K. Diesel based SOFC demonstrator for maritime applications. ECS Trans 2017;78:171–80.
[57] Pasel J, Samsun RC, Tschauder A, Peters R, Stolten D. Water-gas shift reactor for fuel cell systems: Stable operation for 5000 hours. Int J Hydrogen Energy 2018;43:19222–30.
[58] Meißner J, Pasel J, Peters R, Samsun RC, Thimm F, Stolten D. Quantitative analysis of sub-ppm traces of hydrocarbons in the product gas from diesel reforming. Int J Hydrogen Energy 2019;44:4020–30.
[59] Speight JG. Chapter 5 – The Fischer–Tropsch Process. In: Speight JG, editor. Gasification of unconventional feedstocks. Boston: Gulf Professional Publishing; 2014. p. 118–34.
[60] Yoon S, Kang I, Bae J. Effects of ethylene on carbon formation in diesel autothermal reforming. Int J Hydrogen Energy 2008;33:4780–8.
[61] Kang I, Bae J, Bae G. Performance comparison of autothermal reforming for liquid hydrocarbons, gasoline and diesel for fuel cell applications. J Power Sources 2006;163:538–46.
[62] Samsun RC, Peters R. Methodologies for fuel cell process engineering. Fuel Cell Sci Eng: Mater Process Syst Technol 2012:597–644.
[63] Samsun RC, Pasel J, Peters R, Stolten D. Fuel cell systems with reforming of petroleum-based and synthetic-based diesel and kerosene fuels for APU applications. Int J Hydrogen Energy 2015;40:6405–21.
[64] Lehnert W, Lüke L, Samsun RC. High temperature polymer electrolyte fuel cells. In: Stolten D, Samsun RC, Garland N, editors. Fuel cells: data, facts and figures. Weinheim: Wiley-VCH; 2016. p. 235–47.
[65] Pasel J, Wohlrab S, Kreft S, Rotov M, Löhken K, Peters R, et al. Routes for deactivation of different autothermal reforming catalysts. J Power Sources 2016;325:51–63.

Glossary

APU: Auxiliary power unit
ATR: Autothermal reformer
BTL: Experiments using NExBTL diesel
CAB: Catalytic burner
CAD: Computer aided design
CHP: Combined heat and power
$_{el}$: Electric (power)
FTIR: Fourier transform infrared spectrometry
GC: Gas chromatograph
GHSV: Gas hourly space velocity
HEX: Heat exchanger
HT-PEFC: High-temperature polymer electrolyte fuel cell
JA: Experiments using desulphurized Jet A-1
LC: Load change (experiments)
MC: Mixing chamber
MS: Mass spectrometry
$_{N}$: Standard conditions
PEFC: Polymer electrolyte fuel cell
SOFC: Solid oxide fuel cell
$_{th}$: Thermal (power)
ULT: Experiments using Aral Ultimate diesel
WGS: Water-gas shift reactor